Journal of ELECTRONIC MATERIALS, Vol. 50, No. 4, 2021
https://doi.org/10.1007/s11664-020-08477-0

ASIAN CONSORTIUM ACCMS–INTERNATIONAL CONFERENCE ICMG 2020

Magnetocaloric Properties of A-Site-Doped La_2NiMnO_6 for Environmentally Friendly Refrigeration

E. MEHER ABHINAV,[1] D. JAISON,[1] ANURAJ SUNDARARAJ,[1] GOPALAKRISHNAN CHANDRASEKARAN ,[2,4] and S.V. KASMIR RAJA[3]

1.—Nanotechnology Research Centre, SRM Institute of Science and Technology, Chennai, Tamil Nadu 603203, India. 2.—Department of Physics and Nanotechnology, SRM Institute of Science and Technology, Chennai, Tamil Nadu 603203, India. 3.—Directorate of Research, SRM Institute of Science and Technology, Chennai, Tamil Nadu 603203, India. 4.—e-mail: cgknano@gmail.com

La_2NiMnO_6 double perovskite material that simultaneously exhibits both electric and magnetic ordering is used in energy-efficient electronic applications due to its lower power dissipation. The magnetic and electric ordering of Ni and Mn depend on the site occupancy and exchange mechanism driven by the anions, making La_2NiMnO_6 a widely explored material for such studies. The magnetocaloric properties of A-site-doped (Sr^{2+}, Gd^{3+}) double perovskite La_2NiMnO_6 have been investigated experimentally. The synthesized samples showed *Pbnm* orthorhombic symmetry with $P2_1/n$ configuration. The Curie temperature (T_C) of La_2NiMnO_6 (LMN) increased from 277 K to 284 K upon Gd doping due to strong exchange interactions and long-range ordering of Ni^{2+}/Mn^{4+}. Meanwhile, the T_c of LMN was observed to be 268 K upon Sr^{2+} doping, suggesting the possibility of antiferromagnetic ordering. Sr^{2+}-doped (hole-doped) LMN showed lower T_c, magnetic entropy, and relative cooling power (RCP), which may be due to the increase in antisite disorder and exchange bias effect. The chemical stability, tunable transition temperature around room temperature with good control over entropy, wider operating temperature range, and high RCP at lower applied magnetic field make LMN and A-site-doped LMN potential refrigerant materials for use in energy-efficient room-temperature magnetic cooling systems.

Key words: Double perovskite, solid-state refrigeration, entropy change, La_2NiMnO_6 (LMN), magnetic refrigeration

INTRODUCTION

Refrigeration is a major energy-demanding process in the world, and conventional methods for refrigeration pose a great threat to the environment. Consequently, finding solid-state refrigerant systems with higher efficiency that can prevent the use of ozone-depleting gases such as chlorofluorocarbons (CFCs) and hydroclorofluorocarbons (HCFCs) has become critically important. Magnetocaloric cooling systems have attract interest from researchers, particularly for use in room-temperature cooling systems and cryogenics for gas liquefaction. In 1917, Weiss and Piccard discovered the caloric effect for the first time.[1] Giauque and Debye explained how the magnetocaloric effect (MCE) can be used to achieve temperatures in the cryogenic range, and Giauque was awarded the Nobel Prize in 1949 for his contributions to the field of magnetic refrigeration.[2,3] Since that discovery, there has been gradual growth in room-temperature cooling systems over the decades, and notably ambient-temperature cooling systems over the past three decades. The discovery of giant

(Received March 13, 2020; accepted September 9, 2020; published online September 30, 2020)

magnetocaloric materials such as $Gd_5(SiGe)_2$, with first-order transitions at ambient temperature, by Pecharsky paved the way for a large number of research publications in this field since then.[4] These systems exhibit a large magnetocaloric effect and are also highly favorable for use in the magnetic Ericson cycle as their change in adiabatic temperature is almost constant at room temperature. These compounds are considered to represent a major breakthrough in magnetocaloric materials research. Later, Hu et al. found a large magnetic entropy in Heusler alloy (Ni-Mn-Ga) due to the first-order transition, resulting in a great development in magnetic refrigeration.[5] Transition-metal-based compounds such as Mn-As and Mn-Fe-P show a giant magnetic entropy change, comparable to that observed in rare-earth-based intermetallic compounds. The MCE in transition-metal-based compounds is strongly related to the change in magnetization, which in turn greatly depends on the metamagnetic transition and negative lattice expansion above T_c, as reported by Dung et al.[6] The first prototype ambient-temperature refrigerator using the MCE was developed by Brown,[7] and a working model was developed by Astronautics Corporation of America. A maximum entropy change of 8.3 J kg^{-1} K^{-1} at 270 K for a field change of 0 T to 5 T was reported when using perovskite manganite ($La_{1-x}Ca_xMnO_3$) by Andrade et al.[8] Double perovskite oxide has formula $A_2B'B''O_6$, where A is an alkaline-earth metal and B' and B'' belong to the transition metals. In double perovskites, the magnetic and electric ordering of B' and B'' depend on the site occupancy and the exchange mechanism driven by the anions, making them widely studied materials. The effective contribution of magnetic oxides to solid-state cooling applications is yet to be understood completely. Various manganites, perovskites, and double perovskites are being investigated as ambient-temperature magnetic refrigerants[9–17] and have been observed to exhibit a giant MCE, higher chemical stability, low eddy-current heating, and smaller thermal hysteresis than transition-metal- and rare-earth-based alloys, making them a better choice for magnetic refrigeration in various temperature ranges. Related

Table I. Transition temperature, applied magnetic field, maximum entropy change, and RCP of magnetic oxides

Material	Transition Temperature, T_C (K)	Applied Magnetic Field, H (T)	Maximum Entropy Change, ΔS_m (J kg^{-1} K^{-1})	RCP (J kg^{-1})	Ref.
$La_{0.87}Sr_{0.13}MnO_3$	197	5	5.80	232	Ref. 27
$La_{0.80}Ca_{0.20}MnO_3$	230	1.5	5.50	72	Ref. 9
$La_{0.7}Ca_{0.06}Ba_{0.24}MnO_3$	320	1	1.72	44	Ref. 28
$(La_{0.9}Gd_{0.1})_{2/3}Ca_{1/3}MnO_3$	182	1.5	5.78	124	Ref. 29
$La_{0.898}Na_{0.072}Mn_{0.971}O_3$	193	1	1.30	89	Ref. 30
Dy_2NiMnO_6	9.2	7	10.9	295	Ref. 18
Ho_2NiMnO_6	9.6	7	11.4	318	Ref. 18
Er_2NiMnO_6	9.7	7	12.2	267	Ref. 18
Dy_2CoMnO_6	8.5	7	10.5	315	Ref. 19
Ho_2CoMnO_6	17.5	7	11.5	309	Ref. 19
Er_2CoMnO_6	96	7	11.8	259	Ref. 19
Gd_2NiMnO_6	10.5	7	35.5	–	Ref. 20
Gd_2CoMnO_6	6.5	7	24	–	Ref. 20
La_2FeMnO_6	–	5	0.5	–	Ref. 25
$BaLaFeMnO_6$	–	5	0.3	105	Ref. 25
$SrLaFeMnO_6$	–	5	0.3	105	Ref. 25
La_2NiMnO_6 (ordered Single Crystal)	280	7	2.6	206	Ref. 17
La_2NiMnO_6 (dis-ordered single crystal)	170	7	3	–	Ref. 17
La_2NiMnO_6 (thinfilms)	265	7	2	–	Ref. 24
La_2NiMnO_6	260	3	0.98	–	Ref. 31
La_2CoMnO_6	225	5	1.22	–	Ref. 21
$La_{1.95}Sr_{0.05}NiMnO_6$	266	5	1.01	94	Ref. 32
$La_{1.95}Sr_{0.05}CoMnO_6$	210	5	1.35	116	Ref. 32
La_2NiMnO_6	277	1.5	2.81	64.98	Present work
$La_{1.9}Sr_{0.1}NiMnO_6$	268	1.5	2.56	48.6	Present work
$La_{1.9}Gd_{0.1}NiMnO_6$	284	1.5	2.96	67.01	Present work

results for magnetic oxide materials are presented in Table I. Jia et al. found that the magnetic transition temperature is independent of the rare-earth ordering in R_2NiMnO_6 and R_2CoMnO_6, originating only from the Ni^{2+}–O–Mn^{4+} and Co^{2+}–O–Mn^{4+} superexchange interactions, respectively.[18,19] Murthy et al. reported that 3*d*–4*f* interactions can reduce the resultant magnetocaloric effect in double perovskites.[20] La_2CoMnO_6 shows a large specific heat and a broad peak sweeping a wide temperature range, leading to large refrigerant capacity.[21] Balli et al. reported that single-crystal $HoMn_2O_5$ exhibits a giant rotating magnetocaloric effect due to the large magnetic moment of the rare earth Ho^{3+}.[22] Similarly, Chakraborty reported a maximum entropy change for Ho_2NiMnO_6 among the various R_2NiMnO_6 materials (*R* = Pr, Nd, Tb, Ho, and Y).[23] Matte et al. observed table-top-like magnetic entropy variations over a wide temperature range from 100 K to 300 K in La_2NiMnO_6 epitaxial thin films, a compelling system for fabricating magnetocaloric devices.[24] Low magnetization and low MCE were observed by Brahiti et al. in La_2MnFeO_6, $SrLaMnFeO_6$, $BaLaMnFeO_6$, and $CaLaMnFeO_6$ due to antisite cation disorder at *B* and *B′* sites of the double perovskite.[25] In contrast, Ravi et al. observed a high T_C of ∼ 350 K for La_2NiMnO_6 due to oxygen-induced defects and superexchange interactions of Ni and Mn.[26] LMN displays both electric and magnetic ordering at the same time, enabling its use in multifunctional energy-efficient applications. LMN has attracted interest due to its magnetic nature, high electrical resistance, tunability, cost-effectiveness, lower hysteresis loss, high chemical stability, higher transition temperature around ambient temperature, immense entropy change, and broad operating temperature with lower applied magnetic field. These characteristics make LMN a preferable material to study as an ambient-temperature refrigerant material. In the work presented herein, the structural properties and the tunability of T_c by Sr^{2+} hole and Gd^{3+} neutral doping of LMN were studied. The impact of doping on the magnetic phase transitions, magnetic entropy, and magnetocaloric properties of LMN double perovskite oxide were studied to understand the influence of A-site doping of LMN for use in ambient-temperature cooling systems.

EXPERIMENTAL PROCEDURES

LMN was synthesized by using a sol–gel auto-combustion technique. Stoichiometric amounts of high-purity La_2O_3, NiO, and Mn_2O_3 precursors were dissolved in nitric acid. Ethylene glycol (EG) and citric acid (CTA) were added in metal nitrate solution at molar ratio of 5:1:5 (EG:metals:CTA). The final solution was evaporated in a water bath at 400 K until a viscous gel-like product formed. The gels were decomposed by slow heating in air up to 680 K. LMN powder was obtained by calcination of the product at 1473 K for 6 h. Similarly, Gd- and Sr-doped LMN were prepared by substituting 10% of La_2O_3 with Gd_2O_3 or $SrCO_3$ precursor. The microstructure and morphology of LMN were analyzed using a PANalytical high-resolution x-ray diffractometer (XRD) and FEI Quanta FEG 200 field-emission scanning electron microscope (FESEM), respectively. Magnetic properties were studied using a variable-temperature vibrating-sample magnetometer (VT-VSM) at a maximum field of 1.5 T. A set of isothermal magnetization curves [$M(\mu_0 H)$] were acquired by changing the temperature (ΔT) in 4-K steps from 254 K to 294 K, 258 K to 294 K, and 242 K to 278 K for LMN, Gd-doped LMN, and Sr-doped LMN, respectively.

RESULTS AND DISCUSSION

Figure 1 shows the ambient-temperature x-ray diffraction (XRD) patterns of LMN and Gd/Sr-doped LMN double perovskite. The synthesized bulk LMN samples were biphasic with both monoclinic and rhombohedral structure in space group *P121/c1* and *R-3*, respectively, as reported previously.[33] The cell volume and lattice parameters calculated from the XRD data are presented in Table II. It was observed that doping of LMN with Sr or Gd resulted in a slight decrease in the *a*-axis and an increase in the *b*-axis with unchanged *c*-axis, while the cell volume increased in both cases. The tolerance factor (*T*) for LMN and Sr- and Gd-doped LMN was found to be 0.864, 0.871, and 0.863, respectively, indicating perovskite structure. The subtle change in the unit cell parameters of LMN suggests that Gd and Sr ions are compatible with A-site doping. Doping of Gd with relatively smaller ionic radius at A-site of LMN decreases the peak intensity, which is due to point defects affected by the change in electron density.[34,35] Meanwhile, the relative intensity decreased on hole doping with the larger-ionic-radius Sr^{2+} in place of La^{3+}, due to increased scattering centers, increased disorder, and

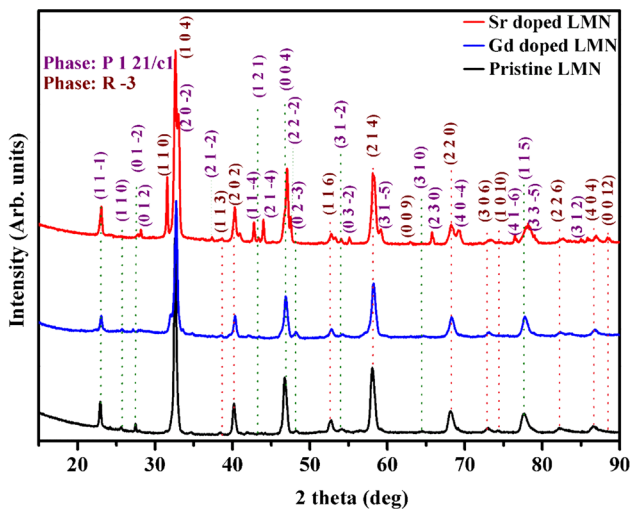

Fig. 1. XRD patterns.

Table II. Structural characteristics of LMN and Gd- and Sr-doped LMN

Bulk Oxide	Crystal Structure (Space Group)	*a* (Å)	*b* (Å)	*c* (Å)	*α* (°)	*β* (°)	*γ* (°)	Cell Volume (Å^3)
LMN	Monoclinic (*P121/c1*)	5.472	5.462	9.443	90	124.64	90	231.58
	Rhombohedral (*R-3*)	5.515	5.515	13.312	90	90	120	350.50
Gd-doped LMN	Monoclinic (*P121/c1*)	5.433	5.532	9.444	90	124.676	90	233.18
	Rhombohedral (*R-3*)	5.515	5.515	13.292	90	90	120	350.11
Sr-doped LMN	Monoclinic (*P121/c1*)	5.432	5.511	9.433	90	124.454	90	232.69
	Rhombohedral (*R-3*)	5.541	5.541	13.303	90	90	120	353.44

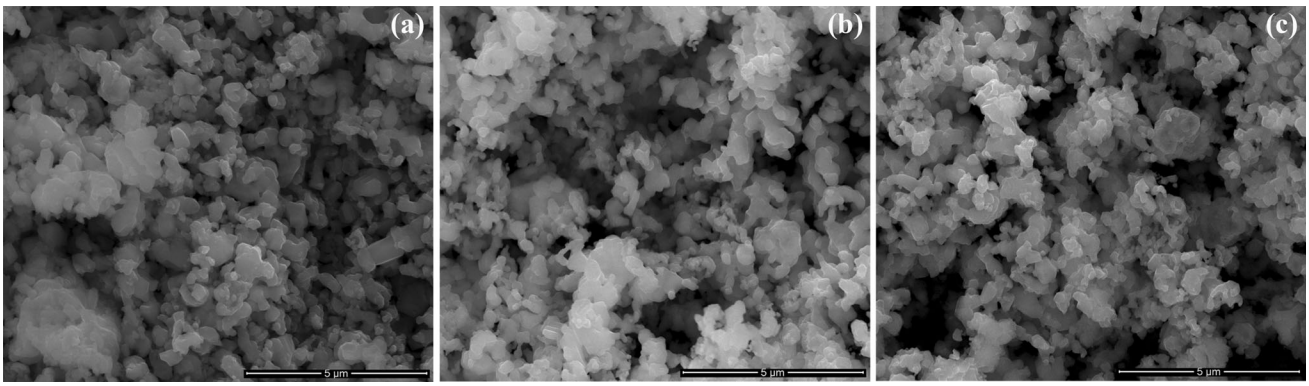

Fig. 2. FESEM images of (a) LMN, (b) Gd-doped LMN, and (c) Sr-doped LMN.

difference in electron density between the atoms. It was also found that the *R-3* phase increased considerably with increasing average valence of Ni/Mn ions, ensuring both Ni and Mn ions were in trivalent state.[36]

The surface morphological characteristics of LMN and Gd- and Sr-doped LMN double perovskites are shown in Fig. 2. The FESEM images revealed a polydisperse nature of the synthesized samples. It was also found that the particles agglomerated to form larger particles.

For MCE analysis, temperature-dependent magnetization M (T) curves of pristine and A-site-doped LMN with an applied magnetic field of 0.5 T were obtained (Fig. 3). Previously, it was observed that LMN with ordered system containing high-spin Ni^{2+} and high-spin Mn^{4+} contributes a ferromagnetic (FM) phase transition at around 280 K, while a disordered system with high-spin Mn^{3+} and low-spin Ni^{3+} results in a decreased transition temperature. Kang et al.[37] carried out field-cooled and zero-field-cooled measurements and observed a decrease in the magnetization with Sr^{2+} doping of LMN, indicating weakening of ferromagnetism and strengthening of antiferromagnetism (AFM). In this study, it was observed that the M (T) curves showed a phase transition from ferromagnetic to paramagnetic behavior at around 277 K, 268 K, and 284 K for pristine LMN and Sr- and Gd-doped LMN, respectively. The T_c of LMN systems is influenced by the ferromagnetic coupling between Mn and Ni ions, which is further influenced by the bond length and bond angle of the structure. The higher T_c for LMN and Gd-doped LMN when compared with Sr-doped LMN is due to the atomic ordering of Ni^{2+} and Mn^{4+} via superexchange interaction, contributing towards the FM state.[33] In Sr-doped LMN, presumably the Ni^{2+}–O–Mn^{4+} FM state is diluted by the Ni^{3+}–O–Mn^{3+} AFM state, resulting in short-range FM order and an increase in the exchange bias (EB) effect, thus lowering T_C.[34] Figure 4 shows the isothermal M–H curves for LMN and Gd- and Sr-doped LMN samples recorded near T_c. The results show a significant decrease in spontaneous magnetization of LMN by Sr doping, whereas it increases with Gd doping. When Sr is doped at A-site of LMN, the magnetization value decreased considerably due to antisite disorder, as reported previously.[37] In the Sr-doped LMN system, the simplification of the magnetization can be attributed to cationic disorder of Ni/Mn arrangement, which is further due to the arbitrary distribution of Mn–O–Ni, Mn–O–Mn, and

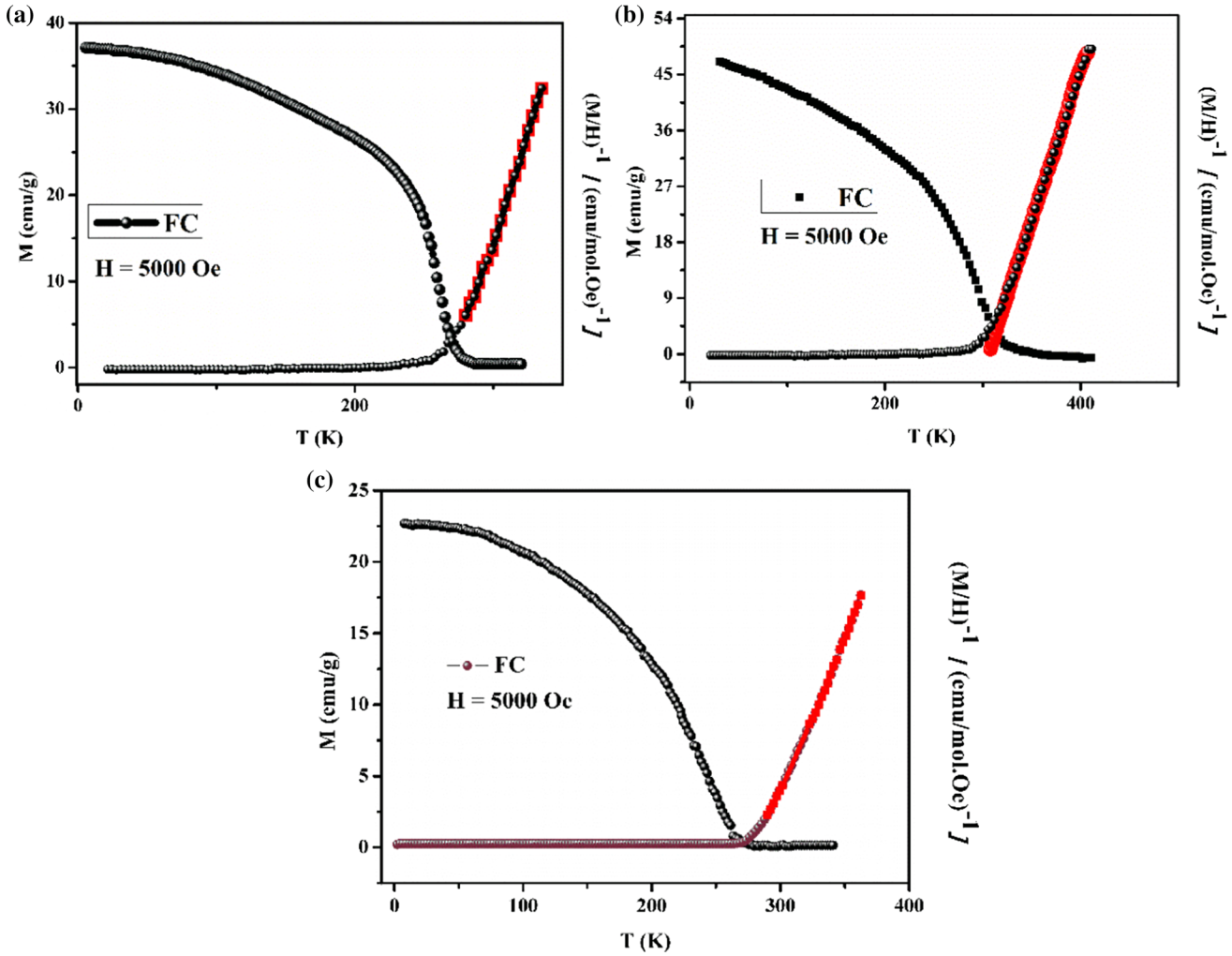

Fig. 3. *M–T* curves of (a) LMN, (b) Gd-doped LMN, and (c) Sr-doped LMN.

Ni–O–Ni bonds. The slope of the magnetization curves increases and magnetic saturation is difficult to attain due to the development of AFM antiphase boundaries (APBs), enhancing the AFM coupling while weakening the FM coupling.[33]

The magnetic entropy change (ΔS_m) values can be obtained from the variable-temperature *M–H* data in the first quadrant. The variable-temperature *M–H* curves for LMN and Gd- and Sr-doped LMN were measured at 242 K to 294 K in steps of 4 K, as shown in Fig. 4. To evaluate the change in entropy of the material, the Maxwell Eq. 1 is used.

$$\Delta S_M(T, \Delta H) = \int_{H1}^{H2} \frac{\partial M(T,H)}{\partial T} H \, dH, \qquad (1)$$

where (ΔS_m) is the magnetic entropy change, and H_2 and H_1 are the final and initial applied magnetic field. The magnetic entropy curves of LMN and Gd- and Sr-doped LMN with an applied magnetic field of 1.5 T are shown in Fig. 5. The calculated $|\Delta S_m|_{Max}$ values at 1.5 T for LMN and Gd- and Sr-doped LMN are ~ 2.81 J kg^{-1} K^{-1}, 2.96 J kg^{-1} K^{-1}, and 2.56 J kg^{-1} K^{-1}, respectively. Due to the high magnetic transition temperature of around 280 K and wide operating temperature range, a large entropy change was observed with a low applied magnetic field. To evaluate the magnetocaloric effect of each material, the RCP is considered in this study, i.e., the product of $|\Delta S_m|_{Max}$ and the full-width at half-maximum (FWHM) of the magnetic entropy curve.

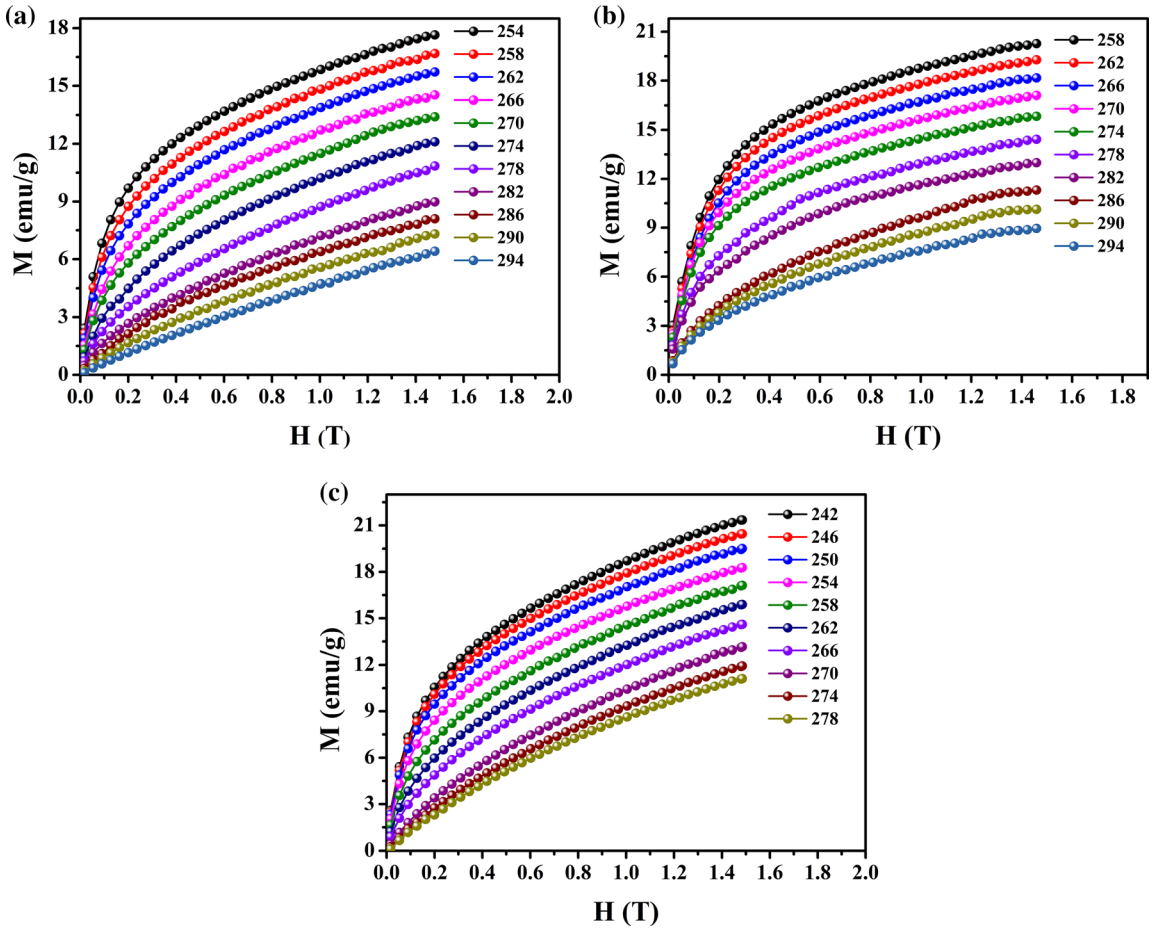

Fig. 4. *M–H* curves of (a) LMN, (b) Gd-doped LMN, and (c) Sr-doped LMN.

The RCP values of LMN and Gd- and Sr-doped LMN at an applied field of 1.5 T was found to be $\sim$ 64.98 J kg^{-1}, 67.01 J kg^{-1}, and 48.6 J kg^{-1}, respectively.

CONCLUSION

The effects of A-site doping on the magnetocaloric properties of double perovskite La_2NiMnO_6 (LMN) were investigated. Structural characterization revealed a biphasic crystal structure, including monoclinic and rhombohedral structures. A transition from ferromagnetic to paramagnetic phase was observed at 279 K, 268 K, and 285 K for pristine LMN and Sr- and Gd-doped LMN, respectively. Gd-doped LMN showed the maximum entropy of about 2.96 J kg^{-1} K^{-1} at 1.5 T and relative cooling power of about 67.01 J kg^{-1}. It was observed that hole doping by Sr^{2+} decreased the T_C, magnetic entropy, and RCP, which may be due to the increased antisite disorder and EB effect. Meanwhile, neutral doping with Gd^{3+} at A-site of LMN was observed to result in a higher T_C, magnetic entropy, and RCP due to B-site cationic ordering. The high resistance to oxidation and corrosion, chemical stability, low cost, wide operating temperature range, and huge RCP with a low applied magnetic field at ambient temperature make LMN and A-site-doped LMN potential candidates for use in room-temperature magnetic refrigeration systems from an application viewpoint.

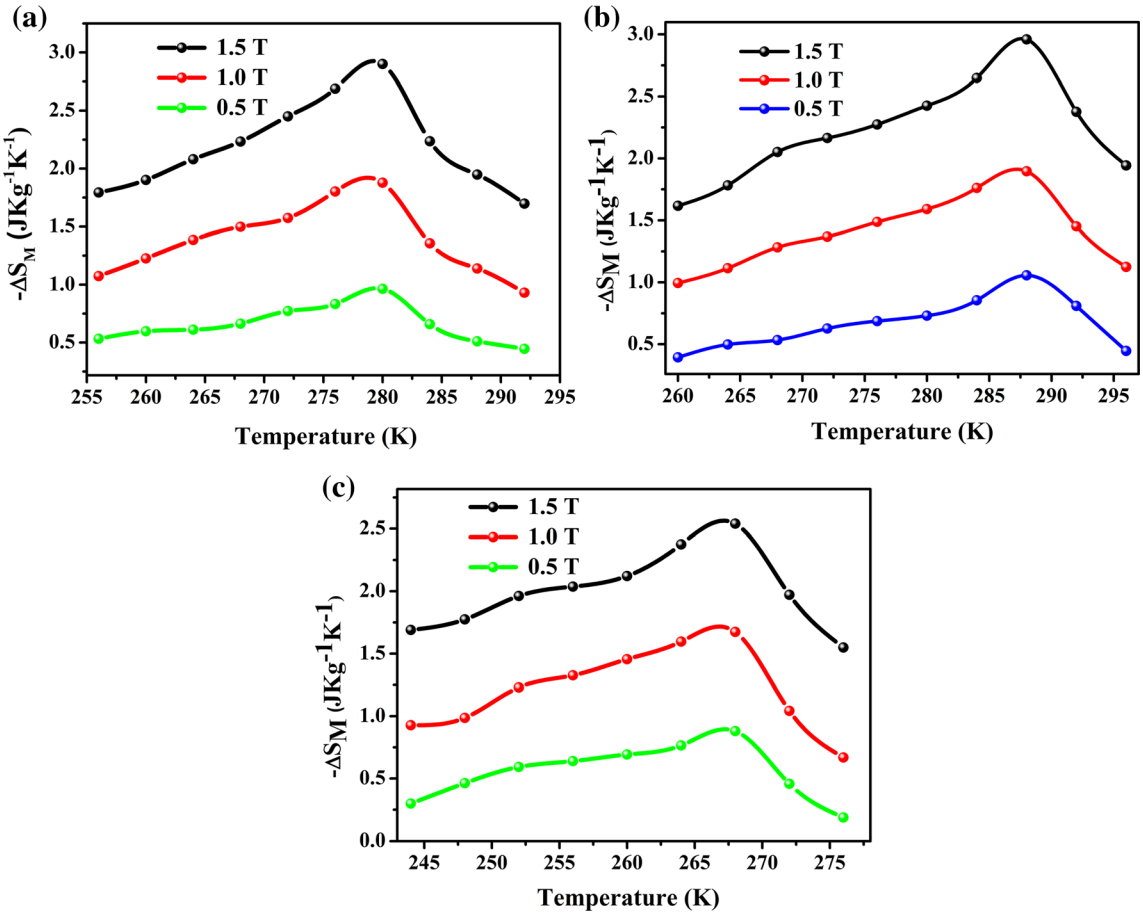

Fig. 5. Entropy curves of (a) LMN, (b) Gd-doped LMN, and (c) Sr-doped LMN.

ACKNOWLEDGMENTS

E.M.A. thanks CSIR India for the fellowship under SRF-Direct Scheme (File No. 09/1045(0013)2K18-EMR). G.C. thanks DST SERB for funding under Grant No. EMR/201, 7/004193.

CONFLICT OF INTEREST

Authors would like to declare that, there are no conflicts of interest to disclose.

REFERENCES

1. P. Weiss and A. Piccard, *J. Phys.* 7, 103 (1917).
2. P. Debye, *Ann. Phys.* 81, 1154 (1926).
3. W.F. Giauque and D.P. Mac Dougall, *Phys. Rev.* 43, 768 (1933).
4. A.O. Pecharsky, K.A. Gschneidner Jr, and V.K. Pecharsky, *J. Appl. Phys.* 93, 4722 (2003).
5. F.X. Hu, B.G. Shen, J.R. Sun, and G.H. Wu, *Phys. Rev. B* 64, 132412 (2001).
6. N.H. Dung, Z.Q. Ou, L. Caron, L. Zhang, D.T. Cam Thanh, G.A. de Wijs, R.A. de Groot, K.H.J. Buschow, and E. Bruck, *Adv. Energy Mater.* 1, 1215 (2011).
7. G.V. Brown, *J. Appl. Phys.* 47, 3673 (1976).
8. V.M. Andrade, R.J.C. Vivas, S.S. Pedro, J.C.G. Tedesco, A.L. Rossi, and A.A. Coelho, *Acta Mater.* 102, 49 (2016).
9. Z.B. Guo, Y.W. Du, J.S. Zhu, H. Huang, W.P. Ding, and D. Feng, *Phys. Rev. Lett.* 78, 1142 (1997).
10. J.Y. Moon, M.K. Kim, and Y.J. Choi, *Sci. Rep.* 7, 16099 (2017).
11. M.K. Kim, J.Y. Moon, H.Y. Choi, S.H. Oh, N. Lee, and Y.J. Choi, *J. Phys. Condens. Matter* 27, 426002 (2015).
12. E.M. Abhinav, A. Sundararaj, D. Jaison, G. Chandrasekaran, M. Krishnan, S. Arumugam, and S.V.K. Raja, *Appl. Surf. Sci.* 483, 26 (2019).
13. A. Kumar, S. Chaudhary, E.M. Abhinav, and R.N. Mahato, *J. Alloys Compd.* 786, 356 (2019).
14. K.A. Gschneidner and V.K. Pecharsky Jr., *Int. J. Refrig* 31, 945 (2008).
15. X. Moya, S. Kar-Narayan, and N. Mathur, *Nat. Mater.* 13, 439 (2014).
16. K.G. Sandeman, *Scr. Mater.* 67, 566 (2012).
17. M. Balli, P. Fournier, S. Jandl, and M.M. Gospodinov, *J. Appl. Phys.* 115, 173904 (2014).
18. Y. Jia, Q. Wang, Y. Qi, and L. Li, *J. Alloys Compd.* 726, 1132 (2017).
19. Y. Jia, Q. Wang, Y. Qi, and L. Li, *Ceram. Int.* 43, 15856 (2017).
20. J.K. Murthy, K.D. Chandrasekhar, S. Mahana, D. Topwal, and A. Venimadhav, *J. Phys. D Appl. Phys.* 48, 355001 (2015).

21. M. Balli, P. Fournier, S. Jandl, K.D. Truong, and M.M. Gospodinov, *J. Appl. Phys.* 116, 073907 (2014).
22. M. Balli, S. Jandl, F. Patrick, and G. Marin, *Appl. Phys. Lett.* 104, 232402 (2014).
23. T. Chakraborty, H. Nhalil, R. Yadav, A.A. Wagh, and S. Elizabeth, *J. Magn. Magn. Mater.* 428, 59 (2017).
24. D. Matte, M. de Lafontaine, A. Ouellet, M. Balli, and P. Fournier, *Phys. Rev. Appl.* 9, 054042 (2018).
25. B. Naima, M. Eskandari, M. Balli, C. Gauvin-Ndiaye, R. Nourafkan, A.M.S. Tremblay, and F. Patrick, *J. Appl. Phys.* 127, 113905 (2020).
26. S. Ravi and C. Senthilkumar, *Mater. Lett.* 164, 124 (2016).
27. A. Szewczyk, H. Szymczak, A. Wisniewski, K. Piotrowski, R. Kartaszynski, B. Dabrowski, S. Kolesnik, and Z. Bukowski, *Appl. Phys. Lett.* 77, 1026 (2000).
28. M.H. Phan, S.B. Tian, S.C. Yu, and A.N. Ulyanov, *J. Magn. Magn. Mater.* 256, 306 (2003).
29. H. Chen, C. Lin, and D.S. Dai, *J. Magn. Magn. Mater.* 257, 254 (2013).
30. W. Zhong, W. Cheng, W.P. Ding, N. Zhang, and A. Hu, *Eur. Phys. J. B* 3, 169 (1998).
31. T.V. Manh, T.A. Ho, T.D. Thanh, T.L. Phan, M.H. Phan, and S. Yu, *IEEE Trans. Magn.* 51, 1 (2015).
32. N. Ouled Nasser, A. Ezaami, M. Koubaa, W. Cheikhrouhou-Kaoubaa, and A. Cheikhrouhou, *J. Mater. Sci. Mater. Electron.* 29, 20658 (2018).
33. N.S. Rogado, J. Li, A.W. Sleight, and M.A. Subramanian, *Adv. Mater.* 17, 2225 (2005).
34. Y. Guo, L. Shi, S. Zhou, J. Zhao, C. Wang, W. Liu, and S. Wei, *J. Phys. D Appl. Phys.* 46, 175302 (2013).
35. R.I. Dass, J.Q. Yan, and J.B. Goodenough, *Phys. Rev. B* 68, 064415 (2003).
36. W.Q. Wang, J.Y. Xiang, K.H. Wu, S.L. Wan, J.J. Zhao, and Y. Lu, *J. Rare Earths* 36, 39 (2015).
37. J.S. Kang, H.J. Lee, D.H. Kim, S. Kolesnik, B. Dabrowski, K. Swierczek, J. Lee, B. Kim, and B.I. Min, *Phys. Rev. B* 80, 045115 (2009).